crystals

MDPI

Article

Application of Organo-Modified Silica Nanoparticles to Improve the Load-Bearing Capacity of Bonded Joints of Dissimilar Steel Substrates

Anna Guzanová [1], Dagmar Draganovská [1,*], Miroslav Tomáš [2], Petr Szelag [3], Nikita Veligotskyi [1], Miroslav Džupon [4] and Marek Vojtko [4]

[1] Department of Technology, Materials and Computer Supported Production, Faculty of Mechanical Engineering, Technical University of Košice, Mäsiarska 74, 040 01 Košice, Slovakia; anna.guzanova@tuke.sk (A.G.); nikita.veligotskyi@tuke.sk (N.V.)
[2] Department of Automotive Production, Faculty of Mechanical Engineering, Technical University of Košice, Mäsiarska 74, 040 01 Košice, Slovakia; miroslav.tomas@tuke.sk
[3] Pragochema spol. s.r.o., Přátelství 550, 104 00 Prague 10—Uhříněves, Czech Republic; vyzkum@pragochema.cz
[4] Institute of Materials Research, Slovak Academy of Sciences, Watsonova 1935/47, 040 01 Košice, Slovakia; mdzupon@saske.sk (M.D.); mvojtko@saske.sk (M.V.)
* Correspondence: dagmar.draganovska@tuke.sk

Abstract: The paper deals with the joining of dissimilar steels by adhesive bonding. The base materials for the experimental work were deep-drawn low-carbon steel DC04, and hot-dip galvanized HSLA steel HX340LAD+Z. Adhesive bonding was performed using rubber-based and epoxy-based adhesives. The research aimed to verify the importance of surface preparation of steel substrates using a formulation with organically modified silica nanoparticles and epoxy organic functional groups, where one end of the functional group can be incorporated into the organic binder of the coating material and the other end can be firmly bonded to substances of an inorganic nature (metals). Since the binder base of adhesives is very similar to that of coatings, verifying the performance of this surface preparation when interacting with the adhesive is necessary. The load-bearing tensile shear capacity of single-lapped joints and the resistance of the joints against corrosion-induced disbanding in a climate chamber were tested. The energy dissipated by the joints up to fracture was calculated from the load-displacement curves. Bonded joints with organosilane were compared with joints without surface preparation and joints prepared by chroman-free zirconate passivation treatment. Exposure of the joints in the climatic chamber did not cause a relevant reduction in the characteristics of the joints. Organosilicate formulation was proved effective when bonding ungalvanized steels with a rubber-based structural adhesive, where it improves the bond quality between the adhesive and the substrate.

Keywords: adhesive bonding; load-bearing capacity of joints; dissipated energy up to fracture

check for updates

Citation: Guzanová, A.; Draganovská, D.; Tomáš, M.; Szelag, P.; Veligotskyi, N.; Džupon, M.; Vojtko, M. Application of Organo-Modified Silica Nanoparticles to Improve the Load-Bearing Capacity of Bonded Joints of Dissimilar Steel Substrates. *Crystals* **2024**, *14*, 558. https://doi.org/10.3390/cryst14060558

Academic Editor: Liqun Li

Received: 30 April 2024
Revised: 5 June 2024
Accepted: 12 June 2024
Published: 17 June 2024

Copyright: © 2024 by the authors. Licensee MDPI, Basel, Switzerland. This article is an open access article distributed under the terms and conditions of the Creative Commons Attribution (CC BY) license (https://creativecommons.org/licenses/by/4.0/).

1. Introduction

The requirements for fuel-efficient vehicles pose a major challenge for engineers to produce lighter and safer vehicles without increasing production costs. An important part of this effort is the use of new lightweight materials in vehicle structures, including high-strength steel, aluminium, magnesium, and polymer composites. A practical example of combining unequal grades of steel is the B-pillar design, where AHSS and mild steel are combined to achieve a compromise between mechanical performance, light weight, and material cost [1,2]. There is a move towards parts composed of different grades and thicknesses of materials, to joining materials of a different material nature (metals + composites), which requires mastery of different joining techniques [3–11]. In joining dissimilar materials, bonding technology holds an important position. Surfaces of different materials differ

not only in morphology but also in surface energy and composition of surface layers and require surface modification to ensure sufficient adhesion of the adhesive. An overview of the different methods of improving adhesive–substrate adhesion is given in Table 1.

Table 1. An overview of the different methods of improving adhesive–substrate adhesion [3–5].

Adhesion Enhancement Method	Characterization	Risk
Degreasing	Removing any loosely held dirt or other contaminants from the surface using solvents	Environmental, health, and safety risks
Machining	Increasing the surface roughness of substrates to enhance mechanical interlocking with the purpose of improving bonding strength	Residual stresses in the new surface; microcrack formation in the surface layer
Abrasion	Removing heavy, loose surface deposits such as dirt, oxide layers, and any other contaminants, increasing the surface area for bonding	Different techniques give different surface morphologies; some techniques may pose certain health hazards; need to get rid of surface dust
Chemical etching	Etching substrates using specific chemicals	Handling with chemicals; different substrates require different etching agents
Chemical primering	Modifying the surface characteristics, increasing the surface energy, and promoting chemical bonding between the adhesive and the substrate (the material being bonded)	Different adhesives and substrates require different primers
Conversion layer formation (phosphating, passivation, and organosilanes)	Application of specific layers to enhance adhesion to various substrates	Complex technological procedure
Physical	Flame treatment, corona discharge, plasma treatment, laser cleaning, laser ablation: these change surface reactivity and modification surface chemistry (polymers) to increase surface energy	Expensive equipment

One of the many methods of improving adhesion is the application of organosilanes [4,12–16]. These are low molecular weight silicon compounds containing at least one Si-C bond. The molecule consists of a core which is aryl or alkyl, one end of the molecule contains an organic functional group providing a strong bond to an organic monomeric or polymeric molecule (rubber, paint, coating, etc.) by binding functional groups, and the other end of the molecule contains an alkoxysilane group forming a strong bond with materials of inorganic nature (metals, minerals, etc.). Thus, the above-mentioned molecules provide a strong bond between organic and inorganic materials, which is useful in coating metals with organic coatings or in bonding metals [17–19].

An extensive study by P. Walker [20] highlighted the potential for the use of organosilanes as adhesion promoters in the organic coating and adhesive bonding of steel and aluminium substrates in a broader context, where improvements in cured bond strength or bond strength under water-soaked conditions are required, pointing out their more pronounced effect when applied in a separate operation as primers rather than when mixed into adhesives as additives.

A. Rattana [21] and J.F. Watts [22] each carried out a very detailed chemical analysis of aluminium alloy surfaces with glycidoxypropyltrimethoxysilane (γ-GPS)-type organosilane, identifying chemisorption and covalent bonds between adhesive and substrate molecules with organosilane using XPS and ToF-SIMS methods.

M.-L. Abel et al. in [23] in their research used the same organosilane (γ-GPS) to treat an aluminium alloy before bonding with epoxy adhesive. They confirmed on experimental joints using XPS and SIMS techniques that the organosilane used forms a kind of diffusion layer with the Al_2O_3 layer on the Al alloy surface, through which the failure zone then

runs when the joint is stressed to peel. A similar detailed analysis by transmission electron microscopy (TEM) and electron energy-loss spectroscopy (EELS) was later carried out by M.J. Whiting [24], confirming the formation of a diffusion layer on Al with a thickness of approximately 70 nm.

His work was followed up by J. Bertho et al. [25], who in his research with the same type of silane (γ-GPS), using TEM and EELS investigation methods, showed that a similar diffusion layer of oxide and silane is formed on the Al alloy surface even when the silane is incorporated directly into the adhesive formulation and applied together with it to the substrate surface.

Boerio et al. in [26] experimented with aminopropyltriethoxysilane (γ-APS) as a primer when bonding steel with an epoxy adhesive. He showed that the pH during silane layer formation has a significant effect on the durability of the joints when exposed to immersion in warm water, and he set the optimum pH value at 8, when the decrease in the mechanical properties of the joints after immersion was the least.

N. Brack and A.N. Rider in [27,28] each experimented with a combination of mechanical, physical, and chemical pretreatment of a Ti-6Al-4V titanium alloy with γ-glycidoxypropyltrimethoxysilane (γ-GPS) on the fracture toughness of joints with rubber-toughened epoxy adhesive as determined by the wedge test. It was shown that a thin organosilane film applied to the titanium slowed degradation rates and led to higher fracture toughness at longer humid-exposure times.

The wedge test was also used by A.N. Rider [28] in testing bonded joints of Al alloys with epoxy adhesive for the aerospace repair industry. He also studied the effect of substrate contamination on its load-bearing capacity as well as the mechanism of moisture penetration at the substrate–adhesive interfacial surface. Similarly, R.A. Gledhill [29] experimented with organosilanes as a primer to prevent atmospheric moisture penetration at the substrate–adhesive interface, which leads to a severe reduction in the load-bearing capacity of the joint and limits the use of structural adhesives in engineering applications.

N. Zoesmar [30] tested the use of organosilanes to improve adhesion between a polymer composite and an additively manufactured AlSi10Mg honeycomb core structure. She found that organosilane increases the surface energy and reduces the contact angle, thus improving surface wettability by the matrix resin.

Organosilanes have also find applications in other areas, e.g., in the dental field. G.J. Han [31] used plasma-enhanced deposition of organosilane and benzene on resin bonded to dental zirconia ceramic. Tetramethylsilane formed a siloxane-like network on the zirconia surface, and benzene provided reactive functional groups that were able to copolymerize with the resin matrix. The result was twice the shear load capacity of the bond compared to commercial zirconia primer.

Y. Guo [32] verified the improvement of the joint load capacity between two composite substrates with PA6 thermoplastic matrix as well as between the composite and Al alloy by the application of γ-GPS silane, identifying Si-O-Si and Si-N covalent bonds responsible for this improvement. An even greater improvement in load-carrying capacity was achieved by a combination of surface roughening and silane application.

The aim of this research was to verify the importance of surface preparation of steel substrates by organosilane with organo-modified silica nanoparticles, which, when applied to the surface by the sol–gel method, forms a network of silicate compounds linked by siloxane bonds with epoxy organic functional groups, which at one end can be incorporated into the organic binder of the coating material and at the other end can be firmly bonded to substances of inorganic nature (metals). Since the binder base of adhesives is very similar to that of coatings, it is necessary to verify the performance of this surface preparation also when it is interacting with the adhesive. The effect of the substrate surface preparation by organosilane is compared with bonded joints without surface preparation and with joints where the substrates were treated with chromium-free zirconate passivation.

2. Materials and Methods

2.1. Base Materials

Two types of steel with a thickness of 0.8 mm were used as the basic material, namely steel type DC04 (W. Nr. 1.0338), hereafter designated as DC and HX340LAD+Z (W. Nr. 1.0933), hereafter designated as HX.

Non-galvanized steel DC is intended for extra deep drawing for car body parts. Hot-dip galvanized high-strength low-alloy steel HX is used for dynamically stressed vehicle parts.

The chemical composition and mechanical properties of the materials used are given in Tables 2 and 3, respectively.

Table 2. Chemical composition of materials, wt. %.

Material	C	Mn	Si	P	S	Al	Nb	Ti	Fe
DC	0.040	0.25	0.009	0.008	0.005	-	-	-	balance
HX	0.07	0.600	0.007	0.016	0.007	0.034	0.025	0.001	balance

Table 3. Mechanical properties of materials (perpendicular to the rolling direction).

Material	Re [MPa]	Rm [MPa]	A80 [%]	Zn Layer [g/m^2]	r	n
DC	197	327	39.0	-	1.900	0.220
HX	414	473	28.4	111	-	-

r—coefficient of normal anisotropy, n—strain hardening exponent.

Due to the mechanical properties of the substrates, it can be expected that a substrate with lower mechanical properties, i.e., DC, may undergo plastic deformation at high joint load-bearing capacities.

The microstructure of DC steel after delivery is shown in Figure 1 and of HX steel in Figure 2.

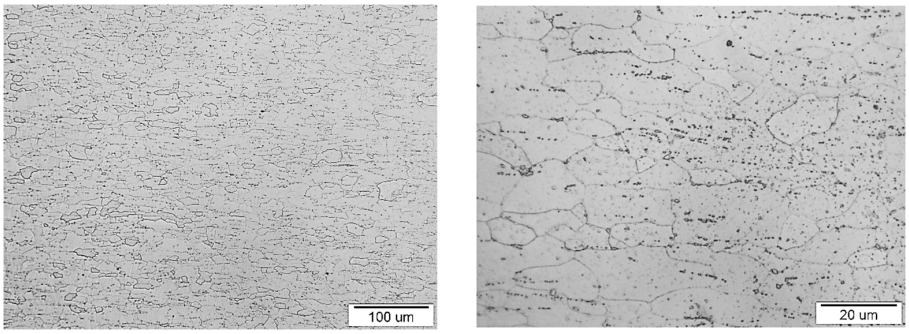


Figure 1. The microstructure of DC steel after delivery, SEM.

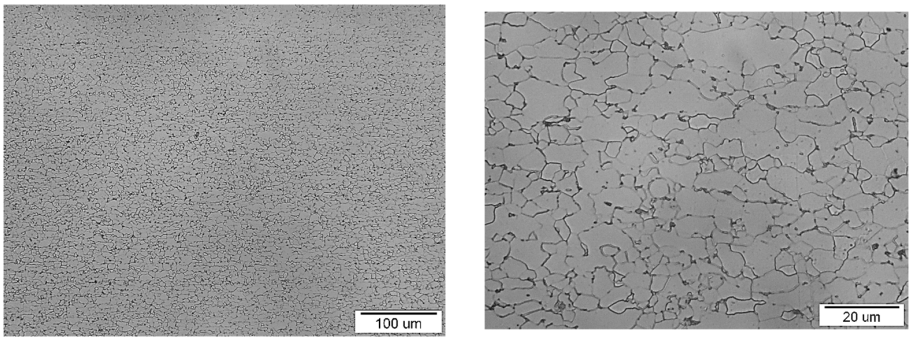


Figure 2. The microstructure of HX steel after delivery, SEM.

DC steel has a fine-grained ferritic structure with very little pearlite (due to the low carbon content), with recrystallized grains slightly elongated in the rolling direction. In addition to the ferritic grains, numerous very small precipitates are visible in the structure. The authors [33] have identified, by SEM and EDS, precipitates in DC04 steels such as calcium silicates and aluminates, which adversely affect the formability of the sheets, but also AlN precipitates, which contribute to the formation of equiaxed grains and, therefore, to the improvement of the formability of these steels [34].

HX steel has a ferritic structure with a small amount of pearlite and with very fine grains due to the addition of niobium.

Since the surface is mainly involved in the bond formation, Figure 3 gives the appearance of the surface as determined by light and electron microscopy.

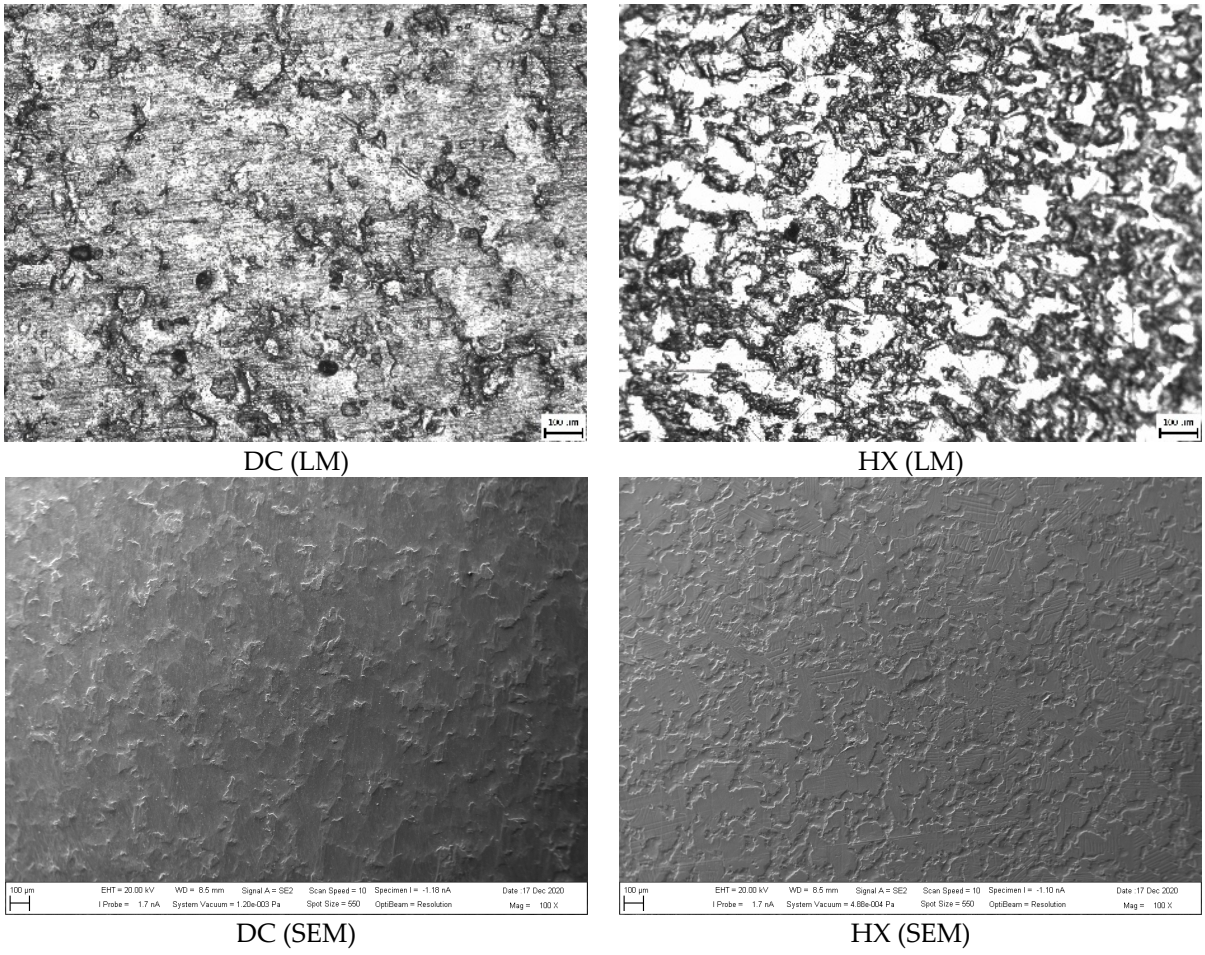


Figure 3. Surface appearance of base materials in as-delivered condition, observed by light (LM) and scanning electron microscopy (SEM).

Figure 3 shows the different nature of the surfaces that will be involved in the formation of the joints. The DC surface is relatively smooth with local peaks and the HX steel surface is relatively smooth with local valleys. Since, in addition to the chemical bonds between the adhesive and the substrate, the mechanical anchoring of the adhesive in the surface irregularities and the extension of the real surface area are also involved in the load-carrying capacity of the joint, the surface of hot-dip galvanized HX steel is more predisposed to form a high-quality joint with a high load-carrying capacity.

2.2. Surface Preparation of Substrates for Bonding

The boundary conditions for the proper functioning of a bonded joint between unequal substrates are determined by the adhesion of the adhesive to the substrates, the cohesive

strength of the adhesive used, and the mechanical properties of the substrates (the load capacity of the joint must not exceed the yield strength of either substrate). While the mechanical properties of the adhesive and the substrates are given, the adhesion to the substrate is a variable that can be influenced just by modifying the surface layers of the substrate.

Three groups of joints were prepared to verify the effect of surface modification of substrates and to compare them with joints on untreated substrates.

One set of joints was made using the substrates in as-delivered condition, without surface preparation. The surface of the steels on delivery was electrostatically oiled with an oil content of about 2 $g \cdot m^{-2}$, and contained common dust particles adhering to the oiled surface, originating from storage and shipping.

A second set of joints was formed on substrates that had been degreased and passivated with a chromium-free zirconate passivation (next: BP). This passivation does not contain any chromium ions or other environmentally hazardous substances. It is used as a conversion passivation layer before coating with organic coatings or before bonding.

A third set of joints was formed from substrates treated with degreasing and experimental preparation with organo-modified silicon nanoparticles at room temperature to increase the adhesion of organic coatings.

The treated steel surfaces were also subjected to SEM analysis to confirm the presence of the formed coatings.

2.3. Methodology of Surface Roughness Measurement of Prepared Surfaces

The roughness of the surfaces of the base materials and modified surfaces was evaluated using a contact profilometer of the Surftest type SJ-201, Mitutoyo, Japan. The roughness of the materials was assessed according to ISO 21920-2. For the analysis of microgeometry, the values that accurately describe the differences in surface roughness were evaluated using the following parameters:

- Ra (arithmetical mean deviation of the measured profile),
- Rz (maximum height of the profile at the basic length),
- RSm (mean width of the element profile),
- non-normalized RPc value (the mean number of peaks per centimetre).

Mean parameter values were calculated from ten measurements performed on each material.

To supplement the description of the surface, profilograms and Abbot Firestone curves were made, representing the material ratio of the profile depending on the particular position of the profile section.

2.4. Adhesives Used and Joint Formation

Two solvent-free adhesives from Henkel production (Henkel AG & Co., KGaA, Dusseldorf, Germany), one rubber-based (hereinafter RB), the other epoxy-based (hereinafter EP), were used for the joints. The basic characteristics of the adhesives are given in Table 4.

Table 4. Basic characteristics of the adhesives.

Adhesive	Type	Colour	E [GPa]	Tensile Strength [MPa]	Shear Strength [MPa]	Elongation at Break [%]	Poisson's Ratio	In-Service Temperature Range [°C]	Curing Conditions
RB	1K	Black	0.880	12	>15	10	0.4	−40 to +90	25 min, 175 °C
EP	1K	Purple	2	35	>30				

The material combinations in adhesively bonded joints were DC-DC, HX-HX, and DC-HX. The shape and dimensions of the test specimens are shown in Figure 4. From the base materials were made single lap joints with bond length 12.5 mm. The adhesive thickness was 0.2 mm.

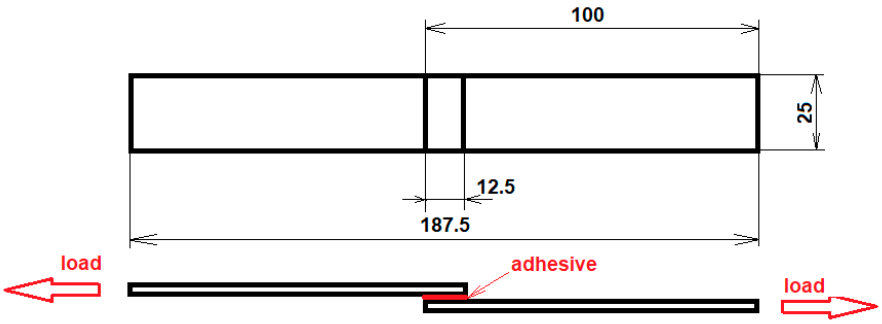


Figure 4. Shape and dimensions of test joint made by adhesive bonding. Thickness of substrate was 0.8 mm, thickness of adhesive layer 0.2 mm. Red arrows indicate testing load.

2.5. Testing of Joints

The joints were cured according to recommendations of adhesive producer and tested for tensile shear capacity in as-bonded condition as well as after the PV1200 corrosion climate test used to test the corrosion resistance of automotive components. In this test, the temperature (from −40 °C to +80 °C) and relative humidity (from 30% to 80%) are cycled, Figure 5. One cycle takes 12 h and, in total, the joints were exposed to 10 test cycles, which took 5 days.

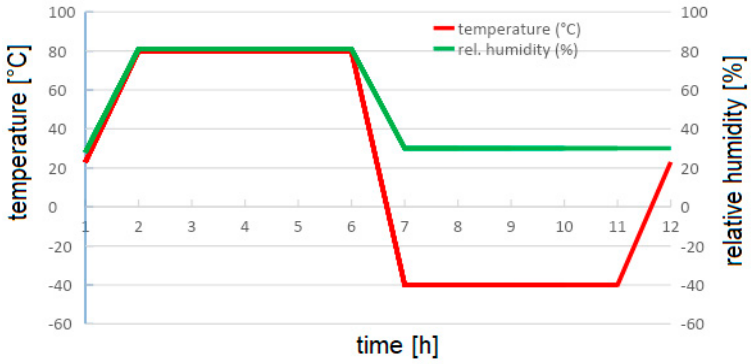


Figure 5. Change in temperature and relative humidity during one cycle in the climate chamber.

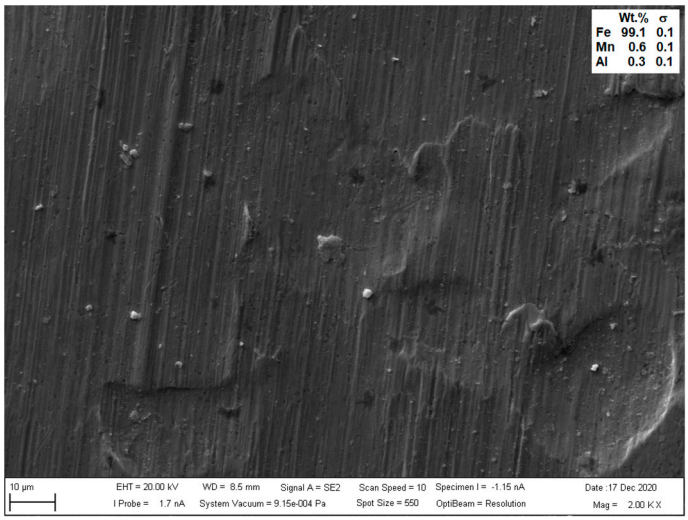
Tensile shear testing of the joints was performed on a universal testing machine TIRA test 2300 (TIRA GmbH, Schalkau, Germany) at a crosshead speed of 10 mm/min. Load–displacement dependence was continuously monitored and data were saved in Excel files. To ensure the reliability of the average load capacity of the joints, 10 joints of each type were tested.

During testing, we observed the load capacity of the joint, i.e., the maximum load on the joint at the moment of failure (Fmax in N) and the displacement when Fmax was reached (sFmax in mm). From the recorded load–displacement dependencies, we calculated the dissipated energy W in J required for failure of the joint as the area under the load curves by trapezoidal integration in Excel.

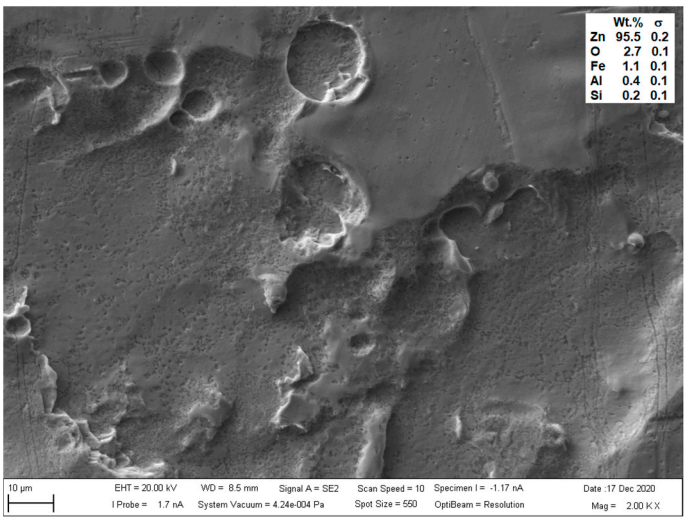
3. Results

3.1. SEM Analysis of Modified Surfaces

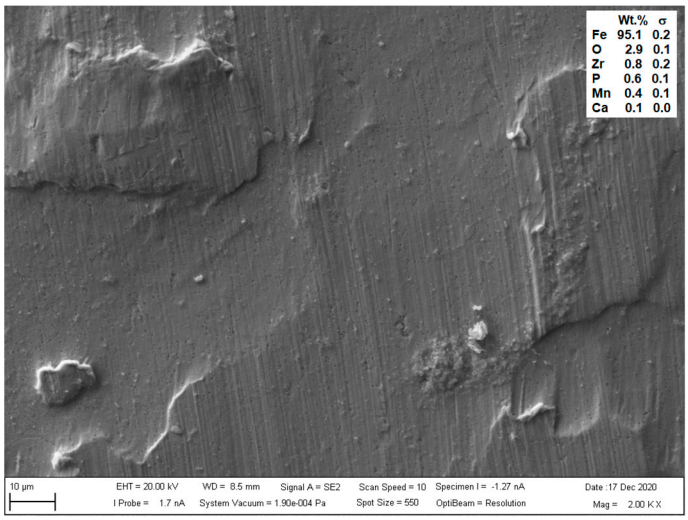
Figure 6 shows SEM images of the surfaces and the corresponding elemental composition of the surface layer.



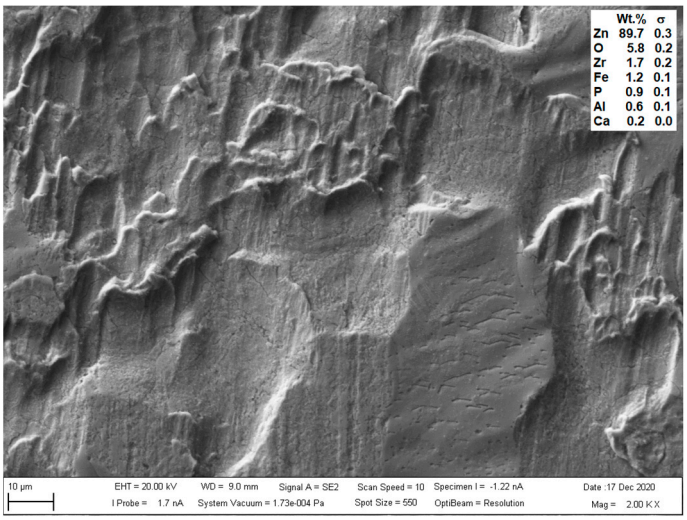
DC as-delivered



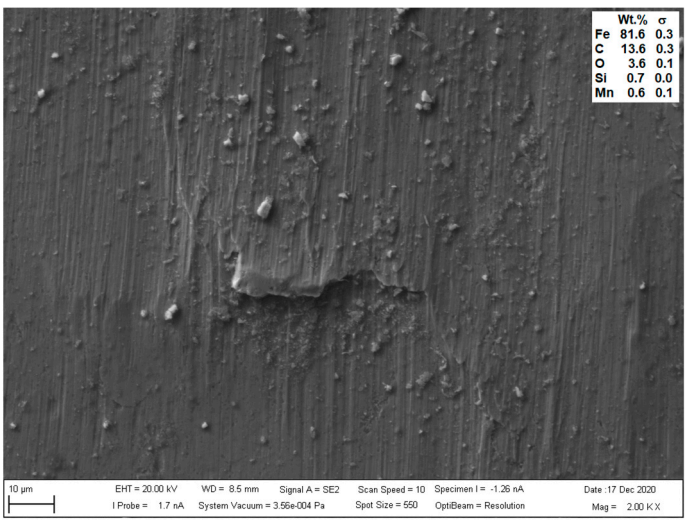
HX as-delivered



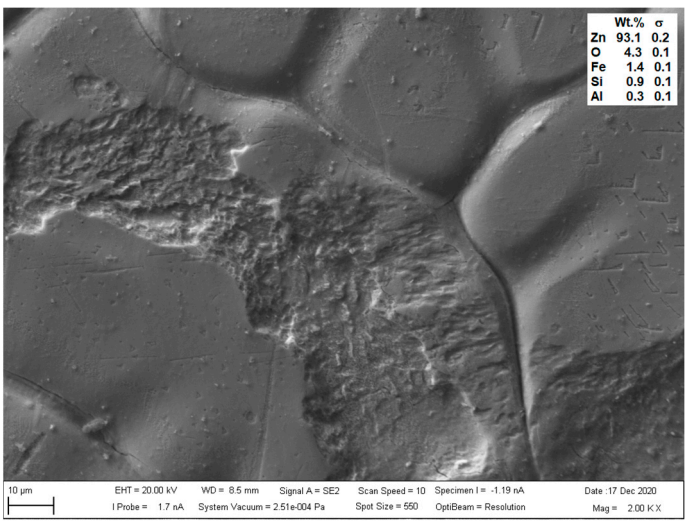
DC BP



HX BP



DC organosilane



HX organosilane

Figure 6. SEM analysis of material surfaces after delivery and after treatment with chromate-free zirconate passivation and organosilane.

From Figure 6 it is clear that the surface treatment with chromate-free zirconate passivation and organosilane did not significantly change the surface morphology; the characteristic features of the surfaces were retained. It follows that the layer of chromium-free zirconate passivation and organosilane is very fine, transparent to light and electron beam, copying the surface, without any morphology of its own. Its presence is only evidenced by EDX spectra. The chromate-free zirconate passivation layer is evidenced by the presence of zirconium in the spectra, and the presence of organosilicate modification is evidenced by the relatively large amount of Si on the modified surfaces. Thus, the surfaces contain the declared layers.

3.2. Results of Surface Roughness Evaluation

The measured values of selected roughness parameters of the surfaces of the base materials in the delivered state and after surface treatments are shown in Table 5.

Table 5. Average values of surface roughness parameters of materials.

	Ra [µm]	Rz [µm]	RSm [µm]	RPc [-/cm]
DC—initial surface	0.93	4.96	240	31.24
DC—passivation	0.96	5.61	238.20	40.15
DC—organosilane	0.95	4.54	249.80	37.17
HX—initial surface	1.02	4.75	135.70	71.12
HX—passivation	0.85	4.67	87.10	109.23
HX—organosilane	0.69	3.98	79.50	115.45

Abbot–Firestone material ratio curves for initial and treated materials are shown in Figures 7 and 8.

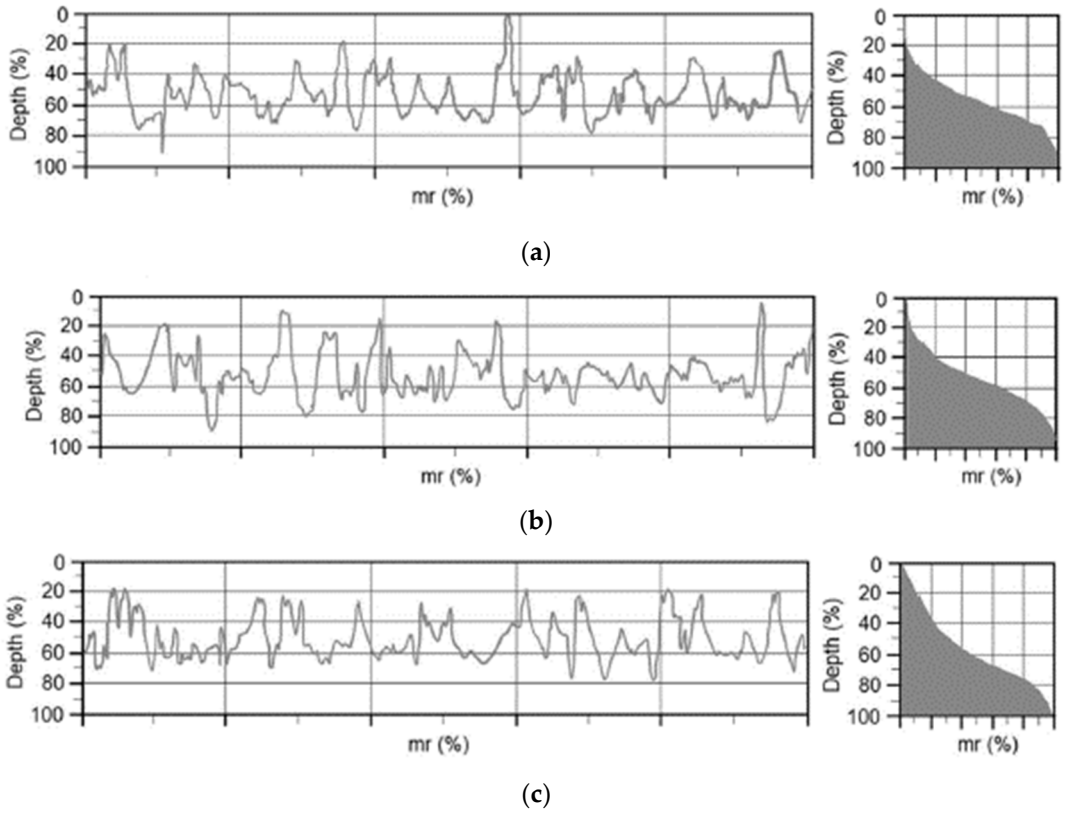


Figure 7. Surface profilograms of materials: (**a**) DC initial surface, (**b**) DC—passivation, and (**c**) DC—organosilane.

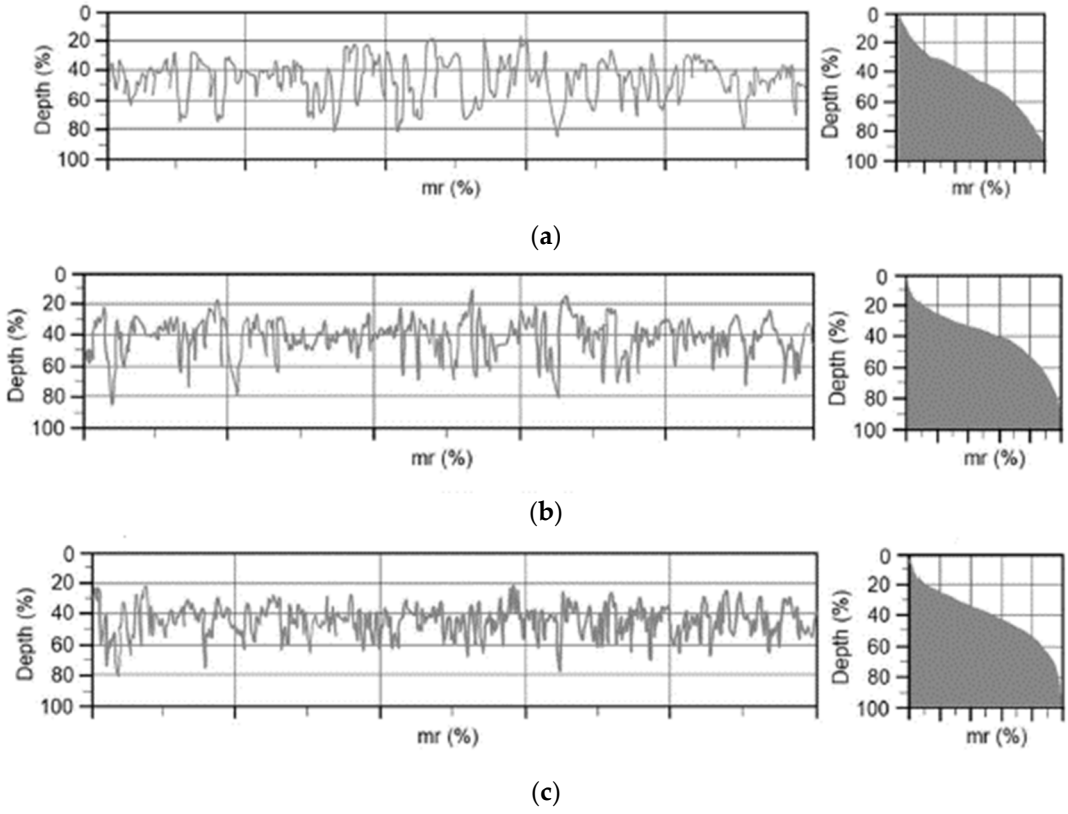


Figure 8. Surface profilograms of materials: (**a**) HX initial surface, (**b**) HX—passivation, and (**c**) HX—organosilane.

The roughness of the evaluated materials was assessed by parameters that would describe the differences in the surfaces. Table 4 shows that the value of the parameter Ra does not change significantly for materials and their surface treatments. It varies for DC material from 0.93 to 0.96 µm and for HX material from 0.69 to 1.02 µm. A similar finding applies to the Rz parameter, as its value ranges from 4.54 to 5.61 µm for DC material and from 3.98 to 4.96 µm for HX material. The differences between the individual surfaces were more pronounced in the RSm and RPc parameters. The number of peaks per centimetre of surface length increased for DC material compared to the original, most obviously on the surface modified by passivation and slightly also on the surface with organosilane.

For HX material, both surface treatments led to an increase in the number of peaks, mostly after the application of the organosilane layer. This fact, specifically the increased number of peaks per centimetre of length, induces an increase in the surface area of the treated surfaces, and thus also an increase in the contact area between the adhesive and the surface-treated material. This could lead to an increase in bond strength.

Differences in surface morphology can be seen in HX materials from profilograms, in Figure 8. This material showed an increase in the number of peaks for both surface treatments compared to the untreated state. However, it is necessary to take into account the fact that the number of peaks in the HX material was double even in its original state compared to DC material, and after modifications the number of peaks is still significantly higher in this HX material compared to DC material with the same modifications (Table 4). The Abbot–Firestone curve is different for both materials in their original state, even though the surfaces have almost the same value for the Ra and Rz parameters. From the mentioned measurements, it can be concluded that from the point of view of microgeometry and the shape of the Abbot–Firestone curve, the HX material and its modified variants are more likely to create a bonded joint with a high load-bearing capacity.

3.3. Load-Bearing Capacity of Joints Formed by Adhesive Bonding

Figures 9 and 10 show the load–displacement curves for adhesive bonding joints formed using equal (DC-DC, HX-HX) and dissimilar (DC-HX) materials, as-joined and also after climate test.

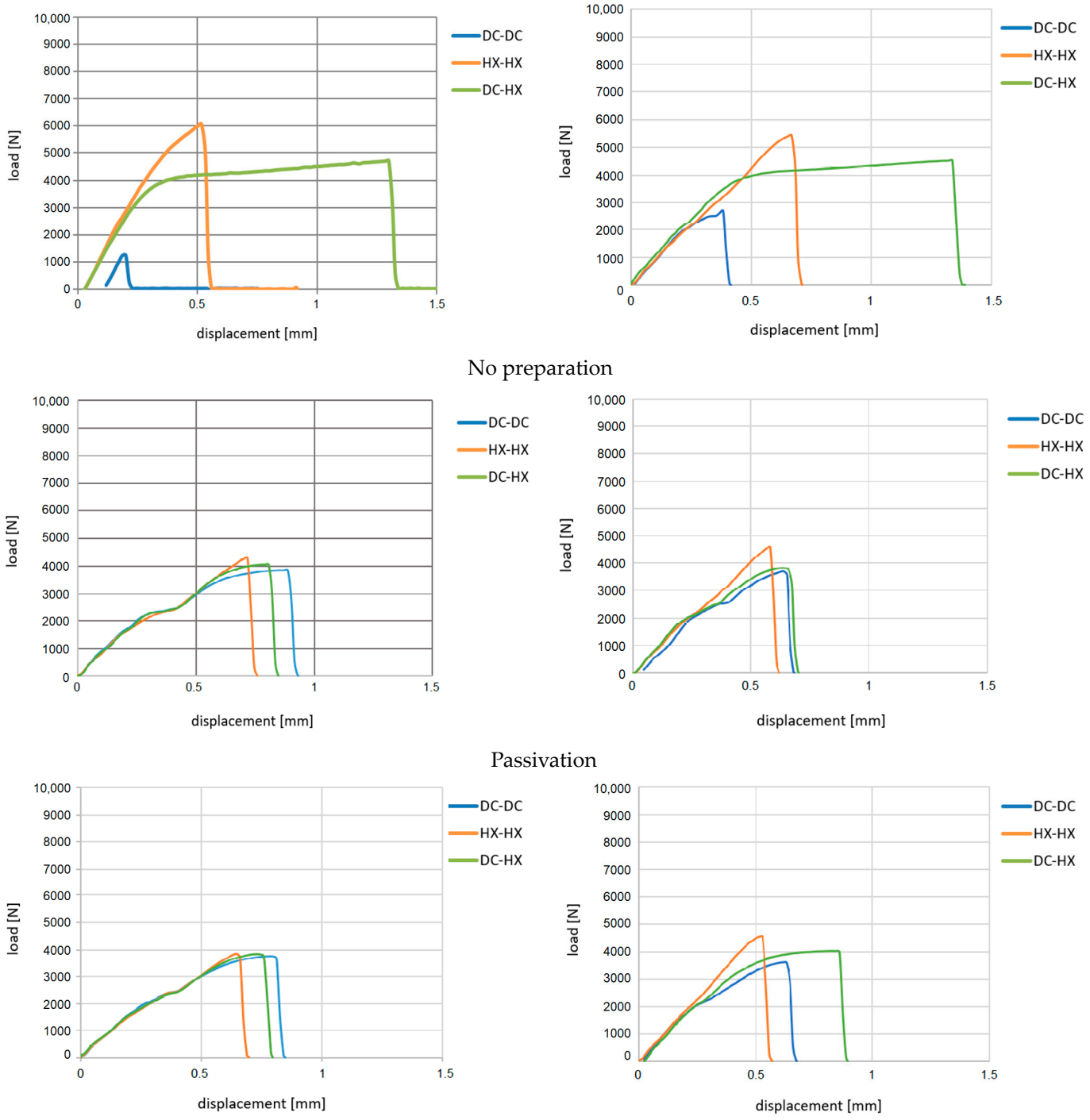


Figure 9. Load–displacement curves of DC-DC, HX-HX, and DC-HX joints for RB adhesive (**a**) as-joined, (**b**) after climate test.

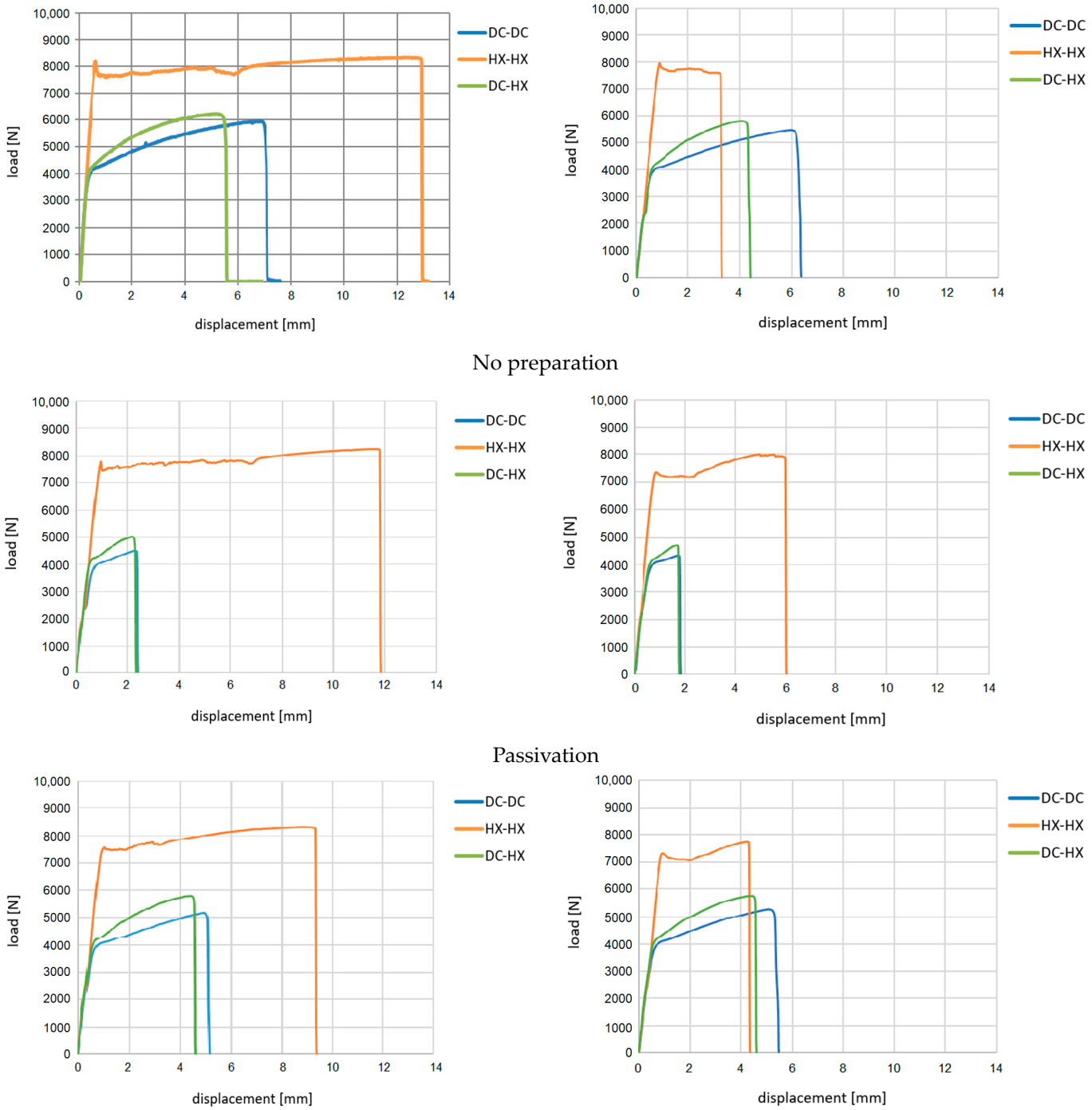


Figure 10. Load–displacement curves of DC-DC, HX-HX, and DC-HX joints for EP adhesive (**a**) as-joined, (**b**) after climate test.

The following findings are evident from Figures 9 and 10:

- RB adhesive joints are characterized by failure occurring after a relatively short displacement (up to 1.5 mm). Joints with EP adhesive fail after deformation of the substrate, after a displacement of 2–13 mm, depending on the joint material combination and surface finish.
- The load-carrying capacity of HX-HX joints is almost always the highest, confirming previous considerations about the more appropriate microgeometry of HX surfaces for

bonding. The load capacity of DC-DC joints is always the lowest among all material combinations evaluated, again reflecting the influence of the microgeometry of this material. The load capacity of DC-HX mixed joints lies logically between that of HX-HX and DC-DC joints, with its Fmax value being closer to that of DC-DC joints. Hence the observation that the load-carrying capacity of joints of dissimilar materials will be significantly affected by the presence of less suitable surface microgeometry.

- The limit state of the bonded joint is not only its failure but also the onset of plastic deformation of one of the substrates. When the bonded joint is working properly, plastic deformation of the substrates should not occur. If we evaluate even the weakest joints (DC-DC) made with RB adhesive from this point of view, their load-bearing capacity is just below 4000 N, which is very close to the force corresponding to the onset of DC yielding (3940 N), which we have determined on the basis of the yield strength of the DC steel (Re_{DC} = 197 MPa) and the cross-section of the DC substrate (0.8 × 25 mm). This shows that the properties of the RB adhesive are utilized as efficiently as possible in the joint; DC-DC joints with RB adhesive fail when the stress in the substrate reaches the yield stress and the substrate strengthening phase begins. The exception is DC-DC joints without surface treatment, which had significantly lower load-carrying capacity. The DC-HX joints behaved similarly, as one of the substrates in the mixed joint is DC and this substrate limits the load-carrying capacity of the joint. The HX-HX joints with RB adhesive have a load capacity very similar to both DC-DC and DC-HX, failing at approximately the same load and displacement value; thus, the load capacity is significantly lower than the yield strength of the HX substrate, which is 8280 N, for Re_{HX} = 414 MPa and substrate cross-section 0.8 × 25 mm. This implies that the joint load capacity of all material combinations (DC-DC, HX-HX, and DC-HX) is approximately the same because it is determined by the cohesion of the RB adhesive itself. If we consider that the shear strength of the RB adhesive itself is >15 MPa (see Table 3) and the overlap area of the joint is 12.5 × 25 mm, the joint should fail at a load of 4680 N or more. Thus, the load-carrying capacity of real joints, which have many imperfections in the performance, actually lies between 3940 N and 4680 N, thus avoiding the onset of plastic deformation of the DC substrate and maximizing the utilization of the RB adhesive properties (in particular, internal cohesion). In the case of the RB adhesive, both surface modifications positively affected the adhesion of the adhesive to the DC substrate. The effect of the surface modification will become more apparent once the absorbed energy of the joints has been quantified.
- DC-DC joints with EP adhesive had a higher load capacity compared with RB adhesive, in that all joints failure occurred only after significant plastic deformation of the substrates. Logically, in this case, there is no point in trying to increase the adhesion of the adhesive to the substrates by some surface treatment. However, for completeness, both surface treatments were also applied and tested with this adhesive (EP). The load-carrying capacity of the HX-HX joints was highest, above the yield strength of the HX material and significantly higher than that of the DC-DC and DC-HX joints. Failure of the HX-HX joints also occurred at a significantly higher displacement value, over a wide region of Luders deformation of the substrate, after the onset of the strain-hardening phase of the HX substrate. The loading behaviour of the DC-DC and DC-HX joints was controlled by the properties of the substrate with lower mechanical properties and less favourable microgeometry, i.e., the DC substrate. These joints failed again in the strain-hardening phase of the DC material, indicating a higher cohesion of the EP adhesive. An EP adhesive with a shear strength > 30MPa and with an overlapped area of 12.5 × 25 mm should fail at a load of 9375 MPa or more, which was never achieved. This means that the joints must necessarily have failed at least partially adhesively (see appearance of joint failure, Figures 11 and 12).
- Surface preparation by chromate-free zirconia passivation had a negative effect on the failure of the joint in terms of a significantly low value of displacement at failure, indicating adhesive failure or disconnection of the passivation layer from the substrate.

Mixed DC-HX joints always have a slightly higher load carrying capacity than DC-DC joints, but fail on a slightly shorter displacement path. In terms of dissipated energy there is probably not much difference between them.

- Corrosion exposure of the joints with EP adhesive in all cases resulted in a reduction of the displacement value at joint failure.

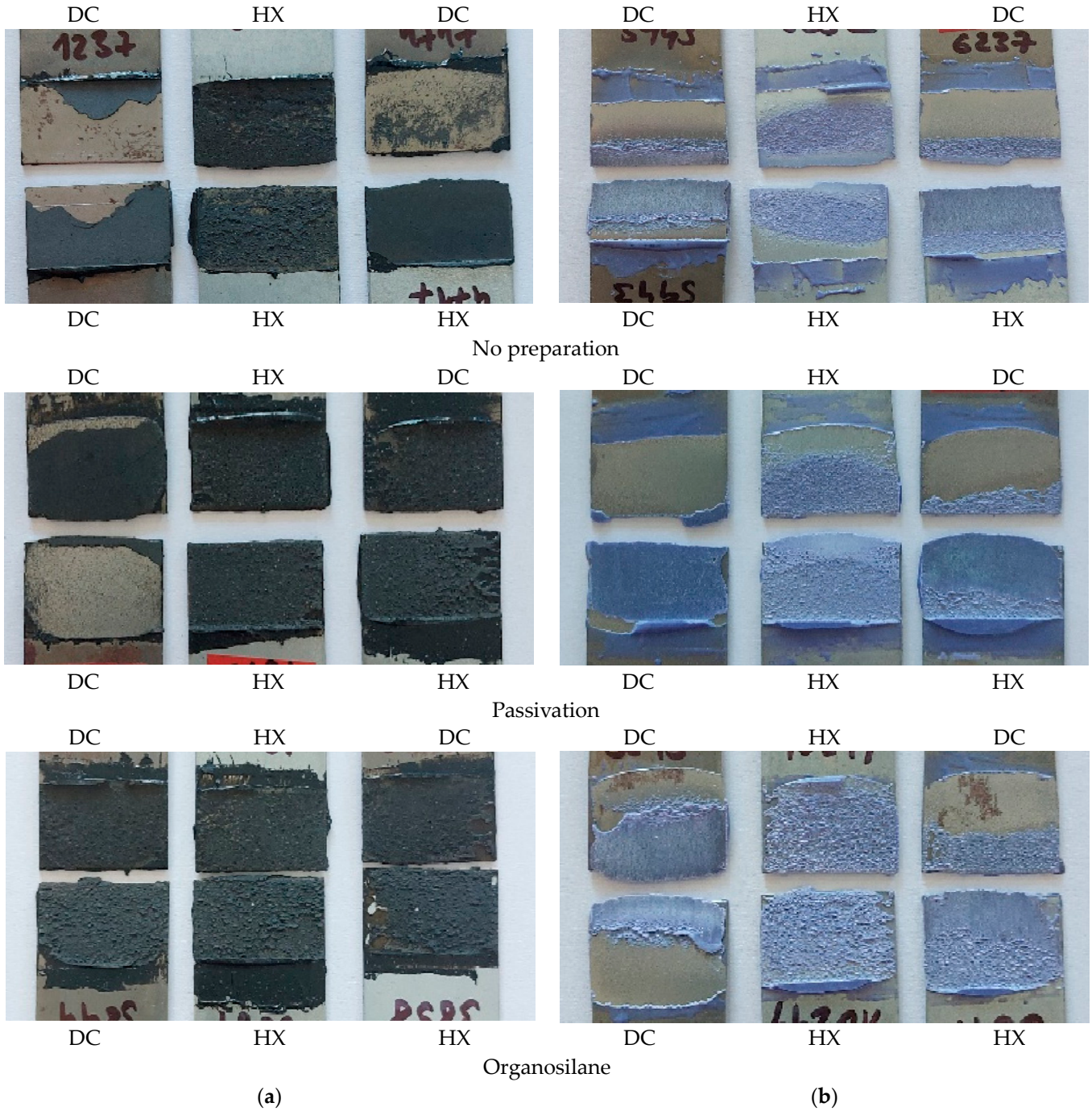


Figure 11. Failure modes of DC-DC, HX-HX, and DC-HX adhesive joints made by (**a**) RB- and (**b**) EP-based adhesives, as-joined.

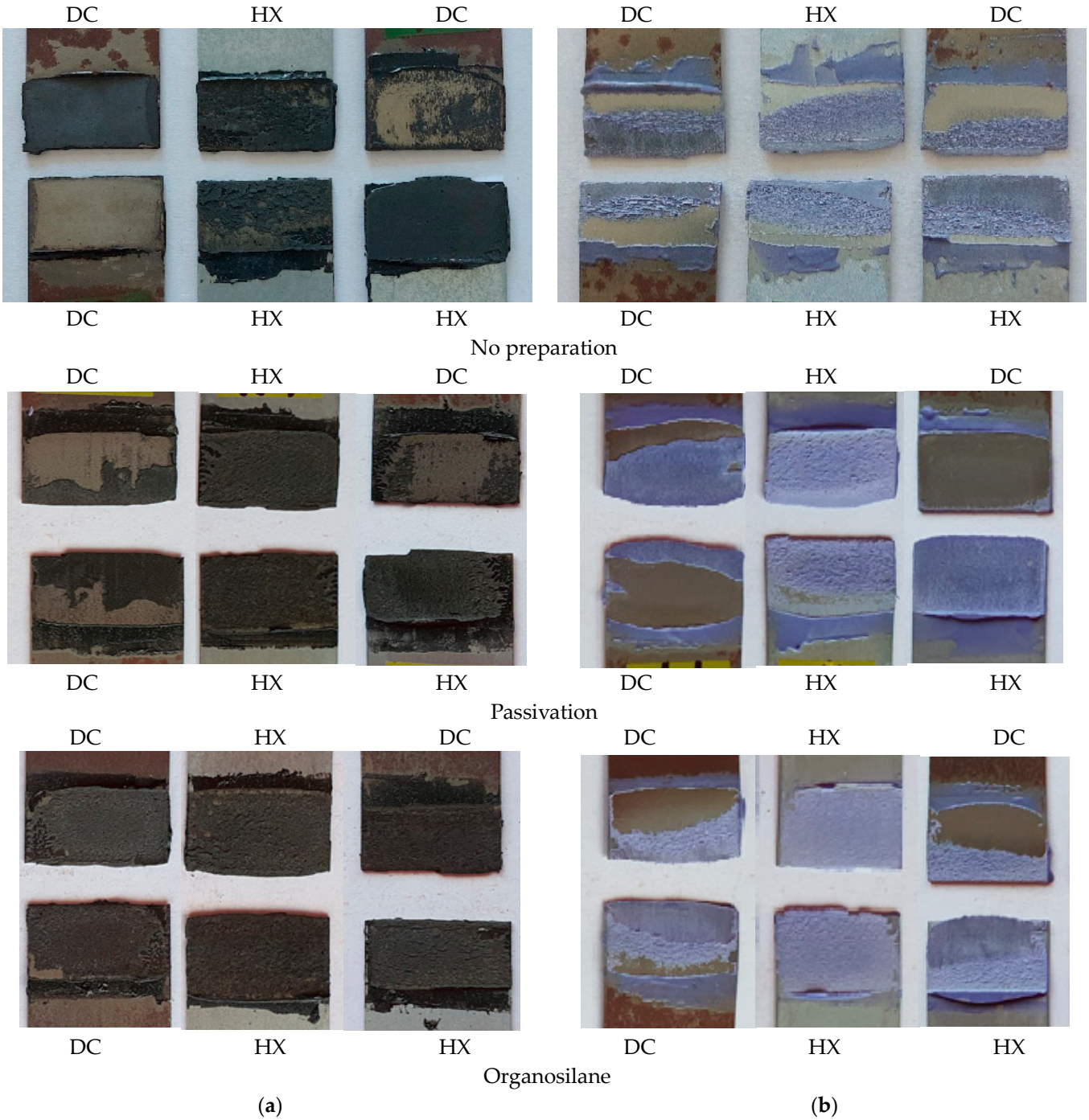


Figure 12. Failure modes of DC-DC, HX-HX, and DC-HX adhesive joints made by (**a**) RB- and (**b**) EP-based adhesives after climate test (CT).

Table 6 summarizes the joint load-carrying capacity Fmax, displacement at joint failure sFmax, and dissipated energy at joint failure W, for both adhesives and all material combinations, during exposure in the climate chamber.

Table 6. Basic load-bearing characteristics of adhesive-bonded joints as-formed and after climate test.

Adhesive	Preparation	Fmax [N]			sFmax [mm]			W [J]		
		DC-DC	HX-HX	DC-HX	DC-DC	HX-HX	DC-HX	DC-DC	HX-HX	DC-HX
RB	no preparation	1237	6054	4717	0.201	0.518	1.299	0.07	1.87	4.96
	passivation	3853	4265	4057	0.874	0.717	0.792	2.34	1.71	2.07
	organosilane	3789	3858	3858	0.787	0.649	0.733	2.02	1.46	1.84
RB-CT	no preparation	2692	5439	4510	0.383	0.669	1.351	0.64	2.02	4.82
	passivation	3714	4617	3828	0.638	0.579	0.632	1.44	1.44	1.63
	organosilane	3621	4558	4018	0.621	0.517	0.819	1.47	1.35	2.42
EP	no preparation	5943	8352	6237	6.823	12.910	5.147	36.17	101.54	29.59
	passivation	4506	8250	5014	2.299	11.786	2.194	8.76	89.62	9.48
	organosilane	5676	8319	6035	7.575	9.342	6.019	36.33	70.96	30.6
EP-CT	no preparation	5454	7596	5804	5.98	3.233	4.313	29.03	21.89	20.93
	passivation	4317	7973	4712	1.714	5.979	1.709	6.25	42.33	6.41
	organosilane	5270	7762	5753	5.334	4.34	4.594	23.96	28.69	22

Figures 11 and 12 show the fracture surfaces of the tested joints, where the type of failure can be noticed: adhesive (between the adhesive and the substrate; one of the substrates is exposed), cohesive (failure in the adhesive layer; the adhesive remains on both substrates involved), or mixed (adhesive–cohesive).

The joint failure surfaces (Figures 11 and 12) confirm the above considerations. The uncoated DC steel has a problem to establish a good bond of the RB adhesive to the substrate. After the DC-DC joint failure, some of the DC substrate remains naked. Both chromate-free zirconia passivation and application of organosilane functional molecules improved the adhesion of the adhesive to the substrate, which was manifested by cohesive bond failure. The HX-HX joints had good adhesion to the substrate independent of surface treatment. For the mixed DC-HX joints, adhesion of the adhesive to HX was excellent regardless of the surface treatment, and adhesion to DC was improved by application of both surface treatments, which was manifested by cohesive failure of the adhesive at the joints with the surface treatment.

The situation is different for the joints formed with EP adhesive; the joints failed at relatively high loads, reaching the plastic deformation region of the DC material when the irregular distribution of shear and peel stress along the bondline became more pronounced. Both of these stresses reach their maximum values at both ends of the bondline, which, together with the higher modulus of elasticity of the EP adhesive (compared to RB), resulted in adhesive failure in at least part of the joint area. But again, weaker adhesion of the adhesive to the DC substrate and better adhesion to the HX substrate is evident. For the EP adhesive, the effect of both surface treatments was not significantly more pronounced.

After exposure of the joints with RB adhesive in the climatic chamber, the joints without surface treatment failed similarly to as-bonded. The effect of surface treatment with chromium-free zirconate passivation decreased in the climatic chamber environment and the joints with this treatment failed adhesively, while the joints with organosilane substrate treatment failed cohesively even after exposure in the corrosive environment. This indicates a very strong bonding of the RB adhesive to the substrate surface (especially DC) via functional groups that prevent moisture penetration and corrosion-induced disbonding.

For the EP adhesive joints after the climatic test, the joints failed in a similar manner to the as-bonded joints; no significant improvement in adhesion was observed due to the surface treatments applied. This only confirms the above observation that for EP adhesive, due to its high load capacity above the yield strength of both substrates, surface modification is of no practical significance to improve adhesive adhesion and increase the load capacity of the joint.

Based on Figures 9–12 and Table 5, after considering the relationships between fracture mechanism, post fracture energy, and post fracture behaviour, we can draw a number of conclusions, outlined below.

Joints made with RB adhesive

The energy dissipated by joints performed on treated substrates upon testing is around 2 J, regardless of the type of failure. Approximately the same value of dissipated energy for both adhesion and cohesion failure means that the adhesion of the adhesive to the treated substrates and the internal cohesion of RB adhesive are approximately the same. So, the surface modifications used only changed the failure mechanism of the joint from adhesive (DC substrate exposure) to cohesive. They did not lead to an increase in the load-bearing capacity or dissipated energy of the joints, but improved the resistance of the joints against corrosion-induced disbonding when exposed in a corrosive environment.

Joints made with EP adhesive

Regarding the joints made with EP adhesive on chemically treated substrates, the adhesion of the adhesive to both types of substrate as well as the cohesion of the epoxy adhesive itself were high, far exceeded the yield strength of the weaker substrate in the joints.

The high cohesion of the epoxy adhesive was most pronounced in the HX-HX joints with good conditions for mechanical and chemical bonding with the adhesive, which was stronger than the cohesion of the adhesive and thus the joints failed by the cohesive mechanism. This was reflected by the highest energy dissipated when the HX-HX joints failed. Since the adhesion of the EP adhesive to the DC substrate was lower, this was evident for all the joints with DC substrate (DC-DC and DC-HX). Pretreatment with zirconate passivation for the DC steel joints resulted in lower Fmax values and earlier onset of failure (displacement value) and thus the dissipated energy is relatively small, compared to organosilane surface preparation. Preparation with organosilane provided higher energy dissipated in DC-DC and DC-HX joints under load, although the limiting factor in mixed joints still remained the adhesion to the DC substrate, which was manifested by the adhesive failure mechanism.

EDX analysis of the fracture surfaces of DC-HX joints and analysis of the adhesive failure mechanism are shown in Tables 7 and 8.

Table 7. SEM analysis of particular areas in joints fracture: RB adhesive.

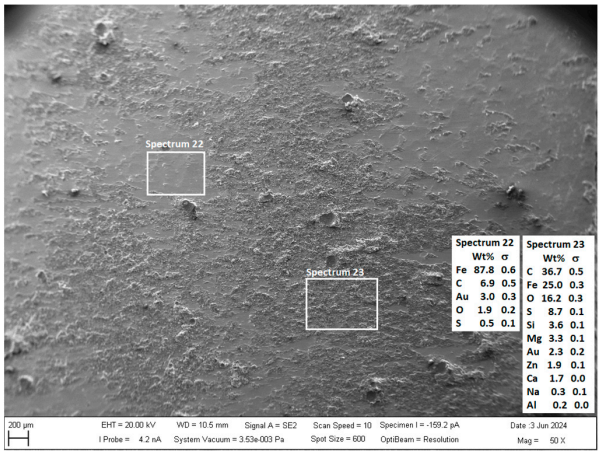
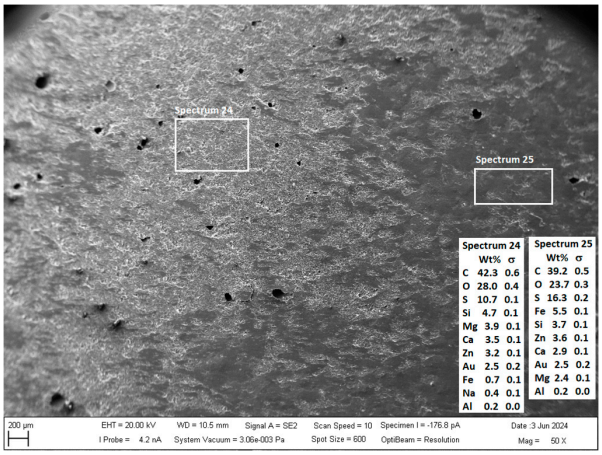
RB	DC	HX
No prep.		

Table 7. *Cont.*

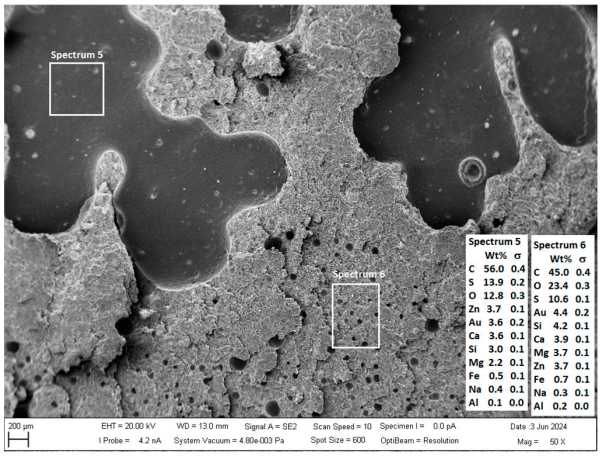
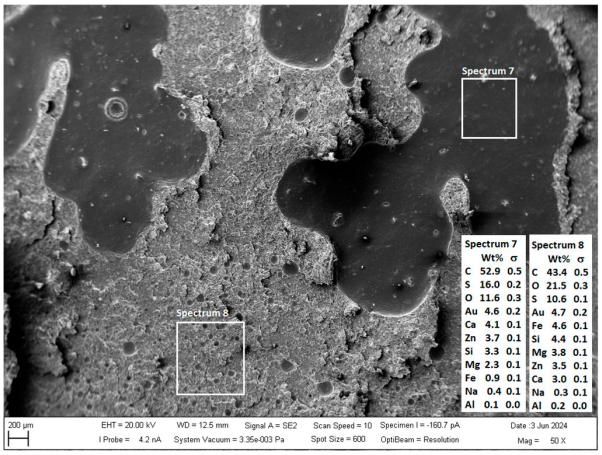
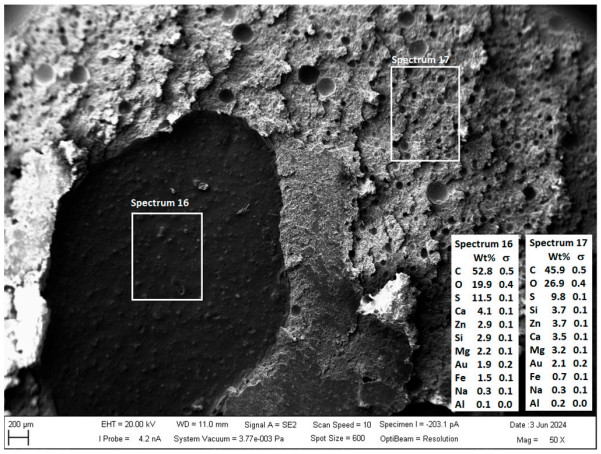
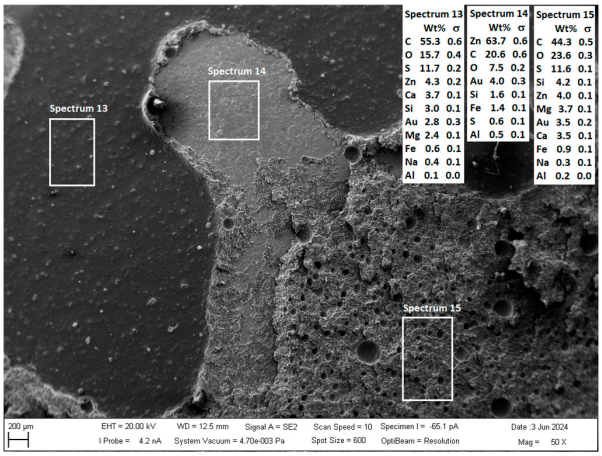
RB	DC	HX
BP		
Org.		

Table 8. SEM analysis of particular areas in joints fracture, EP adhesive.

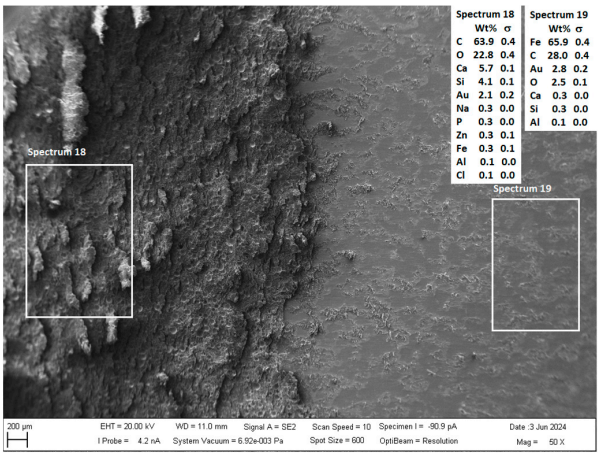
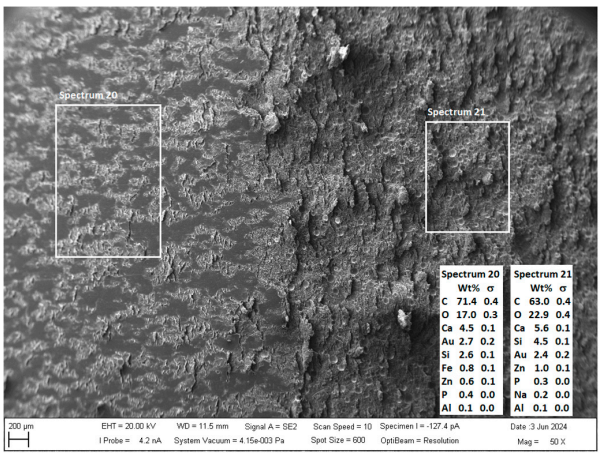
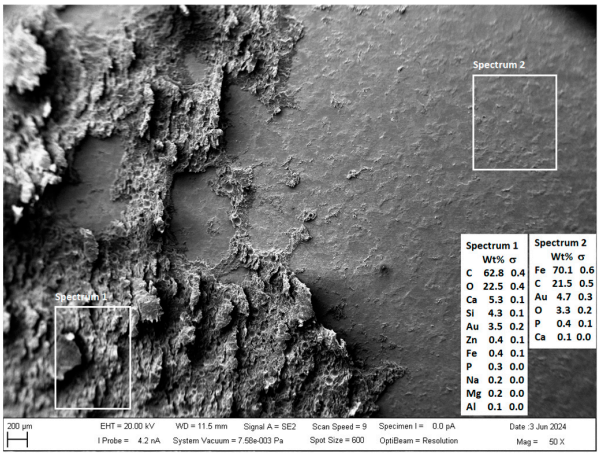
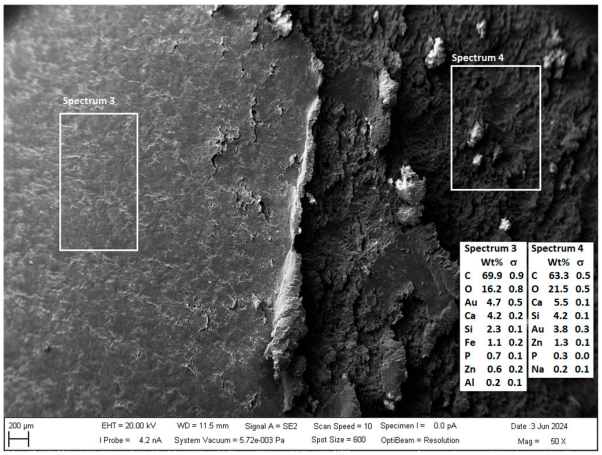
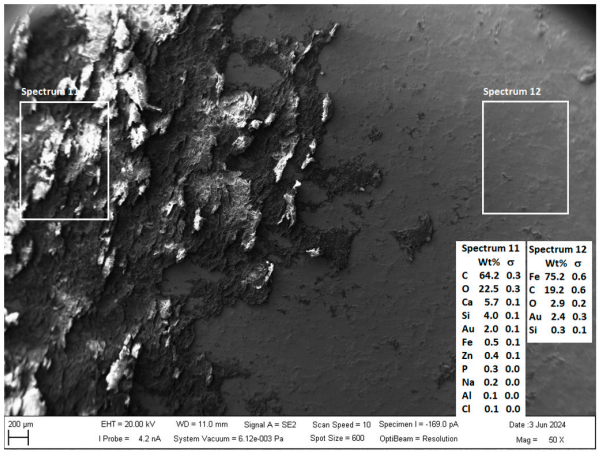
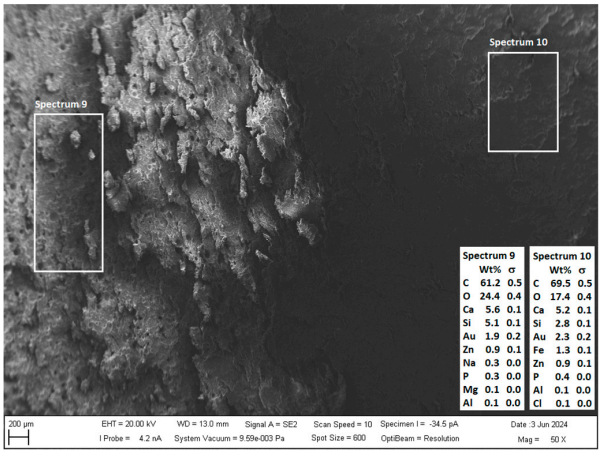
EP	DC	HX
No prep.		

Table 8. *Cont.*

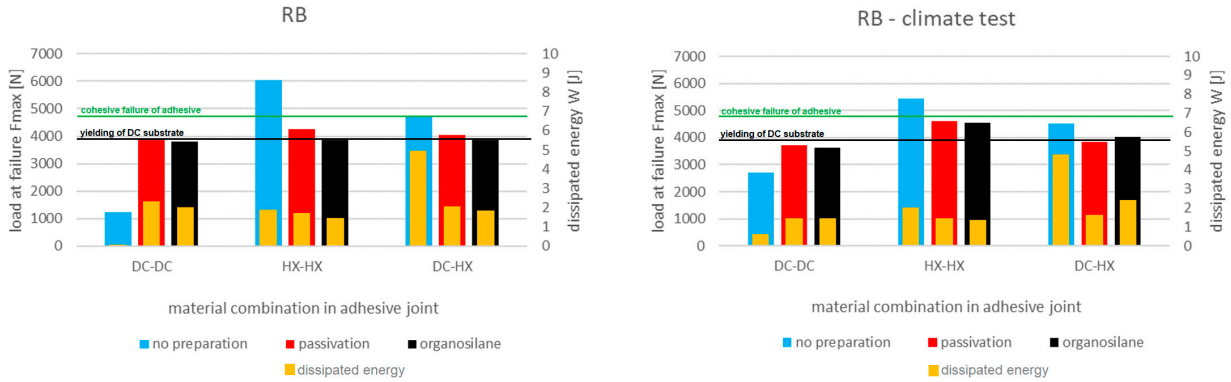
EP	DC	HX
BP		
Org.		

From Table 7 it can be seen on the DC substrate without surface treatment that both exposed (with only a very thin layer of adhesive) and adhesive-covered areas are present; the joint failure is adhesive–cohesive. After treatment with both BP and organosilane the adhesion was improved; the DC substrate remained firmly bonded to the adhesive after the bond failure. The substrate HX without treatment and with the tested treatments is not exposed; RB adhesive is found on it in different thicknesses. The joint failure with the coated substrates is cohesive.

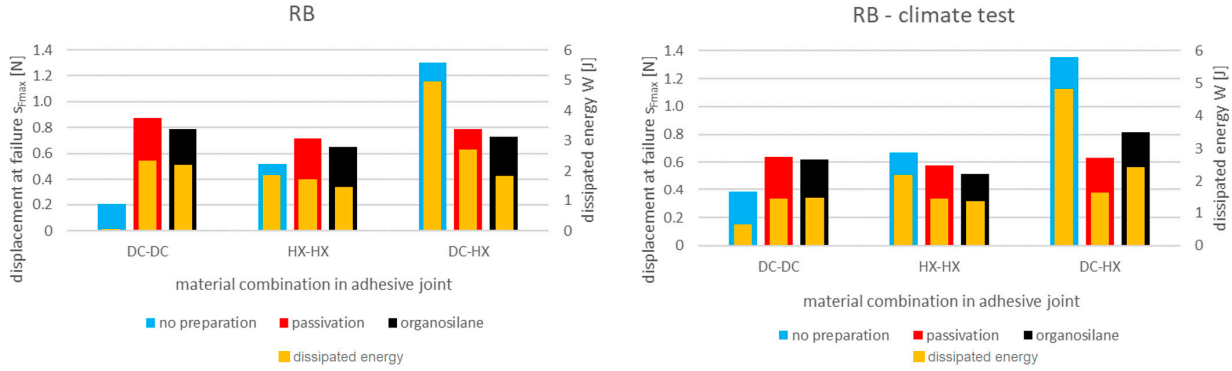
The only exception is the HX substrate, which also contains an exposed site (high Zn content in spectrum 14).

From Table 8 it is clear that DC substrate is revealed in all cases (proved by high Fe content in spectra 19, 2, and 12), but still with a thin adhesive layer (high C content in the same spectra). On the HX steel, there are regions with both thicker and thinner adhesive layers. The small concentration of Fe and Zn in spectra 20, 3, and 10 indicates the presence of an HX substrate under the thin adhesive layer, but no HX substrate was revealed. The bond failure is adhesive–cohesive.

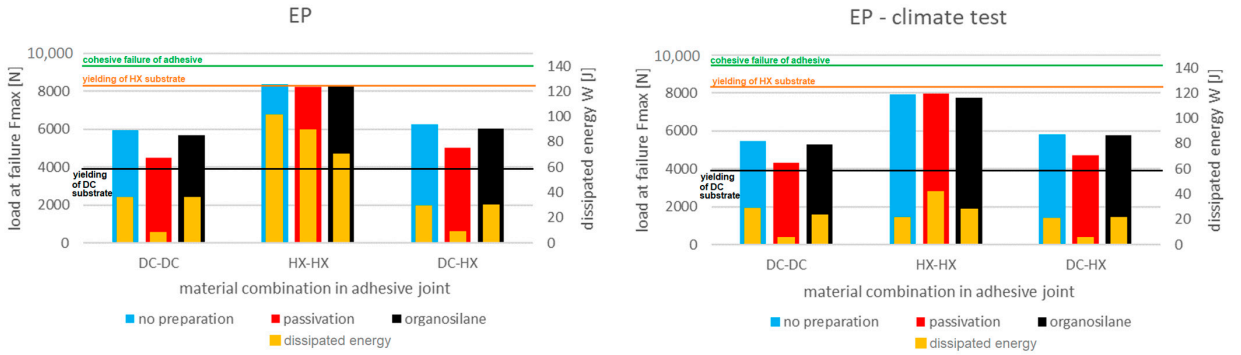
A summary graphical representation of the individual joint characteristics is given in Figure 13.



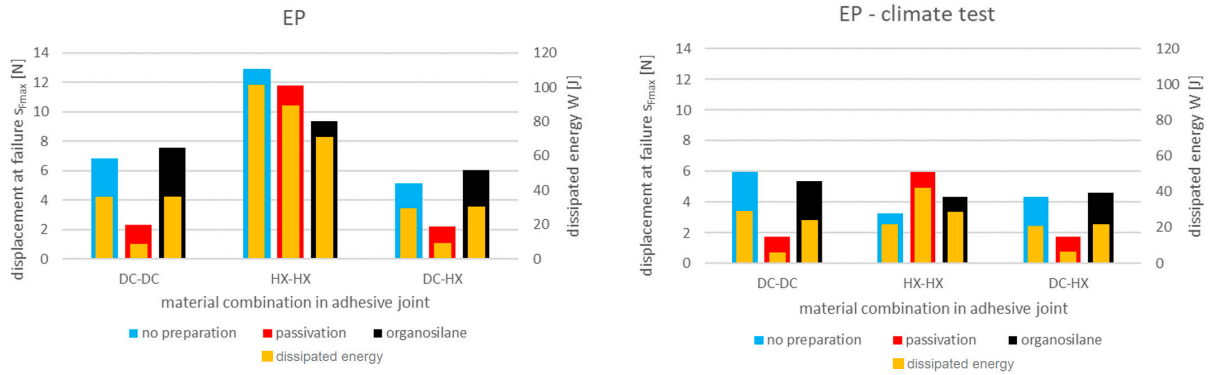
(**a**) RB adhesive, load-bearing capacity versus dissipated energy



(**b**) RB adhesive, displacement at failure versus dissipated energy



(**c**) EP adhesive, load-bearing capacity versus dissipated energy



(**d**) EP adhesive, displacement at failure versus dissipated energy

Figure 13. Load-bearing capacity, displacement at failure, and dissipated energy of the joints.

Figure 13a shows that surface modification of the substrates to form bonded joints with RB adhesive improved the adhesion of the adhesive to the DC substrate and thus brought all the investigated joints (DC-DC, HX-HX, and DC-HX) into the region of optimum utilization of the RB adhesive properties (all Fmax values with surface modification lie between the green and red lines). Joints with RB adhesive and with surface modification fail in the region between the yield strength of the DC substrate and the cohesive shear strength of the adhesive. This improvement in adhesion is maintained even after exposure in corrosive environments.

Figure 13c shows that the surface modification of the substrates was not significant for the formation of bonded joints with EP adhesive, in several cases even leading to a reduction in the load-carrying capacity of the joints, both in terms of Fmax and dissipated energy W; however, all joints, with and without surface modification, lie in the plastic deformation region of the weaker DC substrate in terms of load-carrying capacity, which thus becomes the limiting factor in mixed joints.

Figure 13b,d show the relationship of direct proportionality between the displacement values at Fmax and the dissipated energy at failure W, i.e., the higher the sFmax value, the larger the W value, and vice versa.

4. Conclusions

The following conclusions can be summarized from the experimental work carried out:

- This article presents new findings on sol–gel application of a newly developed formulation with organo-modified silica nanoparticles on degreased steel and hot-dip galvanized steel substrates in order to verify the improvement of the adhesion of two types of adhesives in the formation of bonded joints of identical and dissimilar materials
- In terms of the morphology of the surface involved in the formation and the load-bearing capacity of the joints, the analysis of the microgeometry and the experimentally obtained results showed that the hot-dip galvanized microalloyed steel HX340LAD+Z has a better potential to mechanically anchor the two tested adhesives in the surface compared to the uncoated deep-drawn steel DC04, which, together with the chemical bonds between the adhesive and the surface, will be reflected in the resulting high load-bearing capacity of the joints with this substrate.
- The load capacity of the joints with the rubber-based adhesive was lower than with the epoxy adhesive, but still high enough to maximize the cohesive strength of the adhesive and the elastic deformation of the DC04 substrate.
- The application of the organosilicate formulation is particularly effective when bonding ungalvanized steels with a rubber-based structural adhesive, where it improves the quality of the bond between the adhesive and the substrate, which is manifested by a change from adhesive to cohesive failure when the joint is stressed, and this effect is maintained even when the joint is exposed to a corrosive environment.
- Surface treatment of galvanized steel is not necessary, since the load-bearing capacity of joints with this steel does not improve or deteriorate to the extent that the joint is outside the zone of effective functioning. However, from the point of view of simplicity and efficiency of the technological procedure, it is advisable that the two substrates undergo the surface treatment process together when bonding dissimilar materials.
- The mechanical properties and surface morphology of the weaker of the materials being bonded (in our case, DC04 steel) and its adhesion to the adhesive will be the determining and limiting factor in the load-carrying capacity of the joint and the energy absorbed in the failure of the joint. Therefore, it makes sense to look for other ways to modify the surface of this constituent of the joint.

The application of organosilanes is an interesting promising option to improve the adhesion of organic coatings to metal substrates and increase the load-carrying capacity of bonded joints in a single operation. Moreover, the application of the organosilane layer takes place at room temperature; the bath is not heated, thus requiring no relevant energy

input, and can be incorporated into a commonly established body-coating process without major costs.

Author Contributions: Conceptualization, A.G., P.S. and D.D.; methodology, A.G., P.S., N.V. and M.D.; validation, A.G., D.D. and M.T.; investigation, A.G., N.V., D.D., M.T. and M.V.; writing—original draft preparation, A.G., D.D. and N.V.; writing—review and editing, A.G. and D.D.; project administration, A.G. All authors have read and agreed to the published version of the manuscript.

Funding: This research was supported by project VEGA 1/0229/23: Research on the applicability of thermal drilling technology for the creation of multi-material joints in the automotive industry, KEGA 046TUKE-4/2022: Innovation of the educational process by implementing adaptive hypermedia systems in the teaching of subjects in the field of coating technology and welding of materials and APVV-20-0303 "Innovative approaches in the reconstruction of functional surfaces by laser cladding".

Data Availability Statement: The original contributions presented in the study are included in the article, further inquiries can be directed to the corresponding author.

Conflicts of Interest: The authors declare no conflict of interest.

References

1. Yang, X.; Yao, L.; Yong, X.; Zhou, O. Effect of base steels on mechanical behavior of adhesive joints with dissimilar steel substrates. *Int. J. Adhes. Adhes.* **2014**, *51*, 42–53. [CrossRef]
2. Lamberti, M.; Maurel-Pantel, A.; Lebon, F. Mechanical Performance of Adhesive Connections in Structural Applications. *Materials* **2023**, *16*, 7066. [CrossRef] [PubMed]
3. Luo, J.; Liu, J.; Xia, H.; Ao, X.; Yin, H.; Guo, L. Surface Treatments for Enhancing the Bonding Strength of Aluminum Alloy Joints. *Materials* **2023**, *16*, 5674. [CrossRef]
4. Guzanová, A.; Draganovská, D.; Brezinová, J.; Tomáš, M.; Veligotskyi, N.; Kender, Š. Hybrid Joining of Dissimilar Thin Metallic Sheets—Mechanical Joining and Adhesive Bonding. *Crystals* **2024**, *14*, 220. [CrossRef]
5. Guzanová, A.; Brezinová, J.; Varga, J.; Džupon, M.; Vojtko, M.; Janoško, E.; Viňáš, J.; Draganovská, D.; Hašuľ, J. Experimental study of steel–aluminum joints made by RSW with insert element and adhesive bondings. *Materials* **2023**, *16*, 864. [CrossRef] [PubMed]
6. Messler, R.W., Jr. *Joining of Materials and Structures: From Pragmatic Process to Enabling Technology*, 1st ed.; Elsevier Inc.: London, UK, 2004; p. 815.
7. Messler, R.W. *Joining of Advanced Materials*, 1st ed.; Elsevier Inc.: Stoneham, MA, USA, 1993; p. 539.
8. Alves, L.M.; Dias, E.J.; Martins, P.A.F. Joining sheet panels to thin-walled tubular profiles by tube end forming. *J. Clean. Prod.* **2011**, *19*, 712–719. [CrossRef]
9. Schmerler, R.; Rothe, F. Hybrid Joining Using the Flow Drill Technology. Germany. 2020. Available online: https://www.researchgate.net/publication/341616091_Hybridfugen_durch_Fliesslochformen_Hybrid_joining_using_the_flow_drill_technology#fullTextFileContent (accessed on 10 September 2019).
10. Banea, M.D.; Rosioara, M.; Carbas, R.J.C.; da Silva, L.F.M. Multi-material adhesive joints for automotive industry. *Compos. B Eng.* **2018**, *151*, 71–77. [CrossRef]
11. da Silva, L.F.M.; João, M.; Lopes, C.Q. Joint strength optimization by the mixed-adhesive technique. *Int. J. Adhes.* **2009**, *29*, 509–514. [CrossRef]
12. Moro, R.; Draganovská, D. Monitoring of changes in the roughness of the metal surface after the application of the conversion layer. *Trans Motauto World* **2023**, *8*, 66–68.
13. Bandl, C.; Kern, W.; Krempl, N.; Friesenbichler, W. Simple and rapid method for restoring anti-adhesive organosilane coatings on metal substrates. *Prog. Org. Coat.* **2020**, *140*, 105490. [CrossRef]
14. Li, C.; Liang, T.; Ma, R.; Du, A.; Fan, Y.; Zhao, X.; Cao, X. Superhydrophobic surface containing cerium salt and organosilane for corrosion protection of galvanised steel. *J. Alloys Compd.* **2020**, *825*, 153921. [CrossRef]
15. Liu, T.J.; Sil, M.C.; Chen, C.M. Well-organized organosilane composites for adhesion enhancement of heterojunctions. *Compos. Sci. Technol.* **2020**, *193*, 108135. [CrossRef]
16. Chen, Y.H.; Lai, Y.H.; Wu, P.H.; Chen, L.S.; Lin, Y.S.; Chen, C.M. Mutual intercropping-inspired co-silanization to graft well-oriented organosilane as adhesion promotion nanolayer for flexible conductors. *J. Ind. Eng. Chem.* **2020**, *83*, 90–99. [CrossRef]
17. Campilho, R.D.S.G.; Pinto, A.M.G.; Banea, M.D.; da Silva, L.F.M. Optimization study of hybrid spot-welded/bonded single-lap joints. *Int. J. Adhes. Adhes.* **2012**, *37*, 86–95. [CrossRef]
18. Marques, G.P.; Campilho, R.D.S.G.; da Silva, F.J.G.; Moreira, R.D.F. Adhesive selection for hybrid spot-welded/bonded single-lap joints: Experimentation and numerical analysis. *Compos. Part B* **2016**, *84*, 248–257. [CrossRef]
19. Banea, M.D.; da Silva, L.F.M.; Carbas, R.J.C. Debonding on command of adhesive joints for the automotive industry. *Int. J. Adhes. Adhes.* **2015**, *59*, 14–20. [CrossRef]
20. Walker, P. Organosilanes as adhesion promoters. *Int. J. Adhes. Adhes.* **1991**, *5*, 279–305. [CrossRef]

21. Rattana, A.; Hermes, J.D.; Abel, M.-L.; Watts, J.F. The interaction of a commercial dry film adhesive with aluminium and organosilane treated aluminium surfaces: A study by XPS and ToF-SIMS. *Int. J. Adhes. Adhes.* **2002**, *22*, 205–218. [CrossRef]
22. Watts, J.F.; Rattana, A.; Abel, M.-L. Interfacial chemistry of adhesives on hydrated aluminium and hydrated aluminium treated with an organosilane. *Surf. Interface Anal.* **2004**, *36*, 1449–1468. [CrossRef]
23. Abel, M.-L.; Allington, R.D.; Digby, R.P.; Porritt, N.; Shaw, S.J.; Watts, J.F. Understanding the relationship between silane application conditions, bond durability and locus of failure. *Int. J. Adhes. Adhes.* **2006**, *26*, 2–15. [CrossRef]
24. Whitting, M.J.; Stolojan, V.; Rattana, A.; Watts, J.F. Direct observation and characterisation of the oxide nanostructured interface resulting from organosilane pre-treamtment of aluminium. *MRS Online Proc. Libr.* **2002**, *734*, 18. [CrossRef]
25. Bertho, J.J.; Stolojan, V.; Abel, M.-L.; Watts, J.F. The effect of silane incorporation on a metal adhesive interface: A study by electron energy loss spectroscopy. *Micron* **2010**, *41*, 130–134. [CrossRef]
26. Boerio, F.J.; Williams, J.W. Structure and properties of organosilane primers for adhesive bonding. *Appl. Surf. Sci.* **1981**, *7*, 19–31. [CrossRef]
27. Brack, N.; Rider, A.N. The influence of mechanical and chemical treatments on the envitomental resistance of epoxy adhesive bonds to titanium. *Int. J. Adhes. Adhes.* **2014**, *48*, 20–27. [CrossRef]
28. Rider, A.N.; Olsson-Jacques, C.L.; Arnott, D.R. Influence of adherend surface preparation on bond durability. *Surf. Interface Anal.* **1999**, *27*, 1055–1063. [CrossRef]
29. Gledhill, R.A.; Snaw, S.J.; Tod, D.A. Durability of adhesive-bonded joints employinig organosilane coupling agents. *Int. J. Adhes. Adhes.* **1990**, *10*, 192–198. [CrossRef]
30. Zoesmar, N.; Fuchs, D.; Taha, I. Treatment of additively manufactured AlSi10Mg surfaces for improved bonding with fiber reinforced composites for sandwich applicationsJ. *Sandw. Struct. Mater.* **2022**, *24*, 1152–1168. [CrossRef]
31. Han, G.J.; Kim, J.-H.; Cho, B.-H.; Oh, K.-H.; Jeong, J.-J. Promotion of resin bonding to dental zirconia ceramic using plasma deposition of tetramethylsilane and benzene. *Eur. J. Oral Svi.* **2017**, *125*, 81–87. [CrossRef]
32. Guo, Y.; Li, Y.; Wang, S.; Liu, Z.-X.; Cai, B.; Wang, P.-C. Effect of silane treatment on adhesion of adhesive-bonded carbon fiber reinforced nylon 6 composite. *Int. J. Adhes. Adhes.* **2019**, *91*, 102–115. [CrossRef]
33. Zhang, H.; Wang, Z.; Yang, S. Precipitates and second-phase particles in DC04 steel plate produced by reversible cold rolling. *J. Rechuli/Heat Treat. Met.* **2015**, *40*, 29–34. [CrossRef]
34. Stepien, J.; Burdek, M.; Marcisz, J.; Zak, A.; Janiszewski, J. Microstructure, mechanical properties and geometry of a model batch of semi-spherical steel liners intended for use in the extractive industry. *J. Metallic Mater.* **2021**, *73*, 7–22. [CrossRef]

Disclaimer/Publisher's Note: The statements, opinions and data contained in all publications are solely those of the individual author(s) and contributor(s) and not of MDPI and/or the editor(s). MDPI and/or the editor(s) disclaim responsibility for any injury to people or property resulting from any ideas, methods, instructions or products referred to in the content.